Characterizing viscoelastic properties of breast cancer tissue in a mouse model using indentation

Suhao Qiu [a,b,1], Xuefeng Zhao [a,b,1], Jiayao Chen [c], Jianfeng Zeng [a,b], Shuangqing Chen [d], Lei Chen [e], You Meng [f], Biao Liu [g], Hong Shan [c], Mingyuan Gao [a,b], Yuan Feng [a,b,*]

[a] State Key Laboratory of Radiation Medicine and Protection, School of Radiation Medicine and Protection, Soochow University, Suzhou 215123, China
[b] Center for Molecular Imaging and Nuclear Medicine, School of Radiological and Interdisciplinary Sciences (RAD-X), Soochow University, Collaborative Innovation Center of Radiation Medicine of Jiangsu Higher Education Institutions, Suzhou, Jiangsu 215123, China
[c] Guangdong Provincial Engineering Research Center of Molecular Imaging, The Fifth Affiliated Hospital, Sun Yat-sen University, Zhuhai, Guangdong 519000, China
[d] Department of Radiology, The Affiliated Suzhou Hospital of Nanjing Medical University, Suzhou, Jiangsu 215001, China
[e] Department of Interventional Radiology & Vascular Surgery, The Affiliated Suzhou Hospital of Nanjing Medical University, Suzhou, Jiangsu 215001, China
[f] Department of Surgical Oncology, The Affiliated Suzhou Hospital of Nanjing Medical University, Suzhou, Jiangsu 215001, China
[g] Department of Pathology, The Affiliated Suzhou Hospital of Nanjing Medical University, Suzhou, Jiangsu 215001, China

ARTICLE INFO

ABSTRACT

Breast cancer is one of the leading cancer forms affecting females worldwide. Characterizing the mechanical properties of breast cancer tissue is important for diagnosis and uncovering the mechanobiology mechanism. Although most of the studies were based on human cancer tissue, an animal model is still describable for preclinical analysis. Using a custom-build indentation device, we measured the viscoelastic properties of breast cancer tissue from 4T1 and SKBR3 cell lines. A total of 7 samples were tested for each cancer tissue using a mouse model. We observed that a viscoelastic model with 2-term Prony series could best describe the ramp and stress relaxation of the tissue. For long-term responses, the SKBR3 tissues were stiffer in the strain levels of 4–10%, while no significant differences were found for the instantaneous elastic modulus. We also found tissues from both cell lines appeared to be strain-independent for the instantaneous elastic modulus and for the long-term elastic modulus in the strain level of 4–10%. In addition, by inspecting the cellular morphological structure of the two tissues, we found that SKBR3 tissues had a larger volume ratio of nuclei and a smaller volume ratio of extracellular matrix (ECM). Compared with prior cellular mechanics studies, our results indicated that ECM could contribute to the stiffening the tissue-level behavior. The viscoelastic characterization of the breast cancer tissue contributed to the scarce animal model data and provided support for the linear viscoelastic model used for in vivo elastography studies. Results also supplied helpful information for modeling of the breast cancer tissue in the tissue and cellular levels.

© 2018 Elsevier Ltd. All rights reserved.

1. Introduction

Breast cancer is one of the leading cancers for females, with more appearing new cases than any other cancers (Jemal et al., 2011; Siegel et al., 2016). Understanding and uncovering the biological and physical mechanisms of breast cancer is of great importance for diagnosis and treatment (Ramião et al., 2016). It is known that mechanical properties of cancer tissues are closely related to the cancer pathology and development (Nia et al., 2016; Wirtz et al., 2011). Therefore, mechanical characterization of breast cancer tissues provides crucial information to uncover the mechanobiology mechanism of cancer (Jain et al., 2014; Stylianopoulos et al., 2012). In addition, quantifying the mechanical properties of the breast cancer tissue is also crucial for the construction of accurate physical models, which is needed for building finite element (FE) models (op den Buijs et al., 2011; Pathmanathan et al., 2008). Applications include biomechanical model based precise biopsy of the tumor (Moustris et al., 2011) and image registration (Hipwell et al., 2016). Recently, based on the mechanical properties of the breast cancer tissue, a palpation based automatic diagnosis system has also been proposed (Hosseini et al., 2010). A comprehensive review by Ramião et al. (2016) provides an excellent summary of the current development of biomechanical characterization of the breast tissue.

Several mechanical testing methods have been used to characterize tumor tissues, such as biaxial test (Raghupathy and Barocas, 2010), rheometry test (Wex et al., 2014), and indentation test (Ahn et al., 2010). The biaxial test could provide homogeneous deformations that are ideal for characterizing soft tissues. However, special tissue fixing mechanism is needed that is challenging for small samples (Zhang et al., 2015). Similar problems also exist for rheometry test. However, indentation test has minimum requirements for tissue preparation and has been used to characterize many soft biological tissues such as brain (Budday et al., 2015; Feng et al., 2017b), kidney (Mattice et al., 2006), and meniscus (Han et al., 2017; Li et al., 2017). Therefore, indentation is especially suitable for testing relatively small tissues samples from small animal models. Moreover, the indentation technique is applicable to tissue tests at both macro- and micro- scales (Darling et al., 2006; Park et al., 2004; Toohey et al., 2016). Considering our experiment requirements and sample conditions, we choose indentation test for breast tissue characterization.

Although studies have investigated the mechanical properties of the breast cancer tissue, most of them focused on the elastic properties (Krouskop et al., 1998; Samani et al., 2003; Samani et al., 2007). Using indentation method and a hyperelastic model, Samani et al. (2003, 2007) characterized the elastic modulus of the breast cancer tissue. Using a novel tactile-guided detection device, Mojra et al. carried out viscoelastic characterizations of breast tissue in vivo (Madani and Mojra, 2017; Mojra et al., 2012; Mojra et al., 2011). It has been shown that the measured model coefficient was significantly different between the normal and tumor-included regions (Madani and Mojra, 2017). Nanoindentation of the breast cancer tissue showed the elastic modulus distribution of the tissue could be used to distinguish different cancer types (Plodinec et al., 2012). Magnetic resonance elastography (MRE) (Mariappan et al., 2009; Sinkus et al., 2005) and ultrasound (US) elastography (Chang et al., 2013; Coussot et al., 2009; Han et al., 2016; Ophir et al., 2000) were used to measure the elastic and viscoelastic properties of the breast cancer tissue. However, ex vivo measurements of the viscoelastic properties of the cancer tissue are still needed to guide and validate the tissue modeling. In addition, direct measurements of viscoelastic properties the breast cancer tissue could help biomechanical model based measurements and diagnosis in clinical applications (Griesenauer et al., 2017; Madani and Mojra, 2017).

For the indentation test of soft tissues, elasticity based formulation has been widely applied (Fischer-Cripps, 2000; Mattice et al., 2006; Oyen, 2005). By incorporating the classical elastic solutions with viscoelastic models, a variety of soft tissues were characterized (Budday et al., 2015; Darling et al., 2006; Ning et al., 2006; Qiang et al., 2011; Zhang et al., 2014). Specifically, Prony series based viscoelastic models are the most commonly used for characterizing the viscoelastic properties (Babaei et al., 2015a, 2015b; Wang et al., 2013). Therefore, we used a Prony series based viscoelastic model to characterize the breast cancer tissue.

In this study, we characterize the viscoelastic properties of the breast cancer tissue using a mouse model. To investigate the linear viscoelastic behavior of the tissue that was widely adopted for elastography studies, we compared the mechanical properties of the cancer tissues from two different cell lines at varied strain levels. The morphological structures of the tissue were also analyzed and compared. The results provide detailed viscoelastic characterizations of the breast cancer tissue and a validation for the viscoelastic characterization based on elastography, which could help tissue modeling and cancer diagnosis using biomechanical biomarkers.

2. Materials and methods

2.1. Sample preparation

Twelve healthy female nude mice aged 4 weeks were used in this study. All mice were raised in the Laboratory Animal Center of Soochow University (SPF grade, certificate No. SCXK 2002–0008). The mice were divided into 2 equal groups receiving 2 different tumor cell line injections, respectively. Two typically used breast cancer cell lines, 4T1 and SKBR3 (Shanghai Cell Bank of Chinese Academy of Sciences), were used for tumor implantation. The cells were re-suspended with phosphate-buffered saline (PBS) solutions at a concentration of $10^7 \, \mathrm{mL}^{-1}$. A cell suspension of 0.05 mL was injected subcutaneously into both sides of the rear legs of the mice. The mice were raised for 2–3 weeks until subcutaneous formations of palpable solid tumors with a diameter of 10–15 mm, at least on one of the rear legs (Fig. 1a). Then, the mice were anesthetized by intraperitoneal injection of pentobarbital (50 mg/kg) for surgical removal of the solid tumors. Finally, the mice were euthanized by cervical dislocation after tumor resection. All of the animal procedures and protocols were approved by the Institutional Animal Care and Use Committee of the Soochow University and conducted in accordance with the National Institutes of Health Guide for the Care and Use of Laboratory Animals.

A total of 7 solid tumor samples were harvested for each cell line (Fig. 1b). The sample thicknesses were 4.98 ± 0.55 mm and 3.60 ± 0.50 mm for the 4T1 and SKBR3 samples, respectively. Each sample was put in PBS solutions and transferred to the indentation tester immediately after the resection. The indentation tests were performed at room temperature (∼24 °C).

2.2. Indentation test

A custom-built indentation device was used to measure the viscoelastic properties of the cancer tissue (Fig. 1c). We measured the indentation force and displacement using a load cell (GSO-10, Transducer Technique, USA) and a laser sensor (Model HG-C1050 30 mm, Panasonic, Japan). A linear actuator (43K4U-2.33-A07, Haydon Motion Solutions, Changzhou, China) was used to induce the indentation. The control of the actuator and the data acquisition were accomplished by a data acquisition board (PCI-1706U, Advantech Co., Ltd., China). Samples were placed on top of a translational adjustment unit. A custom-written LABVIEW (National Instruments, USA) program was used for indenter control and data acquisition.

We used a cylindrically shaped indenter with a diameter of 2 mm for the measurement (Fig. 1d). To investigate the linear viscoelastic behavior of the tissue that was adopted in elastography studies, especially MRE (Griesenauer et al., 2017; Sinkus et al., 2005), we indented each sample with five different strain levels that are 2%, 4%, 6%, 8%, and 10%. The indentation depth divided by the sample thickness defined the indentation strain (Feng et al., 2017a, 2017b, 2013). A ramp-hold testing protocol was implemented to characterize the viscoelastic properties (Elkin et al., 2011; MacManus et al., 2016; van Dommelen et al., 2010). In the ramp phase, a strain rate of $\sim 0.1 \, \mathrm{s}^{-1}$ was applied for each strain level. In the hold phase, the indenter was held for a relaxation time of 180 s. The indentation force-displacement data were acquired at a sampling rate of 1 kHz.

2.3. Viscoelastic parameter estimate

For isotropic elastic material, the analytical solution for the flat punch indentation is given by Fischer-Cripps (2000)
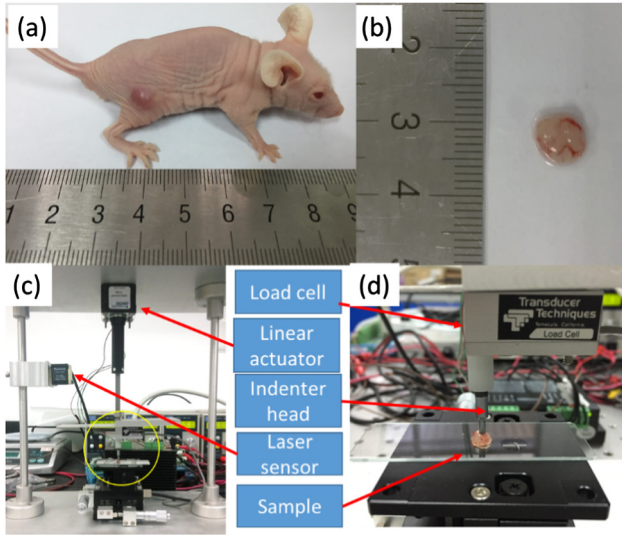
Fig. 1. (a) A solid tumor implanted on the rear leg of a mouse after injection of breast cancer cells intravenously. (b) A tissue sample was prepared from the dissected solid tumor. (c) The custom-built indentation device. The yellow circle is magnified in (d) to show the details of the sample test. (d) Indentation of a sample tissue with a cylindrically shaped indenter. (For interpretation of the references to colour in this figure legend, the reader is referred to the web version of this article.)

$$F = \frac{2ERh}{1 - v^2}, \tag{1}$$

where F is the indentation force, h is the indentation displacement, E is the material elastic modulus, R is the radius of the indenter, and v is the Poisson's ratio. In this study, we assume the tumor tissue is incompressible (Griesenauer et al., 2017; Schierbaum et al., 2017; Tyagi et al., 2017). Therefore, with $v = 0.5$ and $E = 3G$, we have

$$F = \frac{8}{3}ERh = 8GRh, \tag{2}$$

where G is the shear modulus.

In order to compensate the infinite half space assumption of the model, we adopted the Dimitriadis model for the bounded condition (Dimitriadis et al., 2002)

$$F = 8GRh(1 + 1.133\chi + 1.283\chi^2 + 0.769\chi^3 + 0.0975\chi^4), \tag{3}$$

where $\chi = \frac{\sqrt{Rh}}{H}$, H is the thickness of the sample. In this formulation, the bounded equation was adopted since no slippery was observed between the sample and the substrate. For the ramp-hold indentation protocol, the indentation displacement h is a piecewise function of t

$$h(t) = \begin{cases} Vt & (0 \leqslant t \leqslant t_R) \\ h_{max} & (t_R \leqslant t) \end{cases}, \tag{4}$$

where V is the indentation velocity and $h_{max} = Vt_R$ is the maximum indentation depth.

Using the correspondence principle of viscoelastic materials, we used a 2-term Prony series $G(t)$ to substitute for the elastic shear modulus G

$$G(t) = C_0 + \sum_{i=1}^{2} C_i e^{-\frac{t}{\tau_i}}, \tag{5}$$

where C_0, C_i, and τ_i are model parameters. The instantaneous shear modulus G_0 and long-time shear modulus G_∞ can be computed

$$G_0 = G(0) = C_0 + \sum_{i=1}^{2} C_i, \quad G_\infty = G(\infty) = C_0 \tag{6}$$

Apply the generalized Boltzmann integral for indentation under displacement control (Oyen, 2005), with Eqs. (3) and (5) we have

$$F = 8RX \int_0^t G(t - u) \frac{dh}{du} du = \begin{cases} 8RXV \int_0^t G(t - u)du & (0 \leqslant t \leqslant t_R) \\ 8RXV \int_0^{t_R} G(t - u)du & (t_R \leqslant t) \end{cases}, \tag{7}$$

where $X = (1 + 1.133\chi + 1.283\chi^2 + 0.769\chi^3 + 0.0975\chi^4)$, t_R is the indentation ramp time, u is the dummy variable for the integral. The analytical solution for F can be derived by substituting the indentation displacement function h using Eq. (4):

$$F = \begin{cases} 8RXV\left(C_0 t - \sum_{i=1}^{2} \tau_i C_i \left(e^{-\frac{t}{\tau_i}} - 1\right)\right) & (0 \leqslant t \leqslant t_R) \\ 8RXV\left(C_0 t_R + \sum_{i=1}^{2} \tau_i C_i e^{-\frac{t}{\tau_i}}\left(e^{\frac{t_R}{\tau_i}} - 1\right)\right) & (t_R \leqslant t) \end{cases}, \tag{8}$$

Both the ramp and relaxation sections of the piecewise function were used for parameter estimate. The objective function used for optimization is

$$f_{obj}(C_0, C_i, \tau_i) = \left[w_1 \sqrt{\frac{1}{n} \sum_{j=1}^{n} (F^j - F_{exp}^j)^2}\right]_{0 \leqslant t \leqslant t_R}$$
$$+ \left[w_2 \sqrt{\frac{1}{m} \sum_{k=1}^{m} (F^k - F_{exp}^k)^2}\right]_{t_R \leqslant t} \quad (i = 1, 2, 3). \tag{9}$$

An equal weight for the ramp and relaxation sections was taken arbitrarily, where $w_1 = w_2 = 0.5$ are the weighting ratios. n and m are the data points acquired from the ramp and relaxation section, respectively. The optimization was achieved by a custom-written MATLAB code using function "fmincon" (MathWorks, Natick, MA, USA).

2.4. Histology and statistical analysis

To observe the morphological differences of the two different tumor tissues, we stained the tissues with hematoxylin and eosin (H&E). Briefly, samples were immersed in 10% paraformaldehyde, transferred to 70% ethanol, and embedded in paraffin wax blocks. Before staining, tissue sections with a thickness of 8 μm were transferred to a glass slide and dewaxed in xylene, rehydrated through decreasing concentrations of ethanol, and washed with PBS. Finally, sections were dehydrated through increasing concentrations of ethanol and xylene for observation (Gang et al., 2009).

We analyzed the morphological structures of the tissues by estimating the volume ratio of the nucleus ($\phi_{nucleus}$) and all the other contents without the nucleus (ϕ_{cell}). The two ratios were estimated by evaluating the percentage of corresponding fractional area in a fixed field of view (FOV) in one stained slice,

$$\phi_{nucleus} = \frac{A_{nucleus}}{A - A_{gap}}, \quad \phi_{cell} = \frac{A_{cell}}{A - A_{gap}}, \tag{10}$$

where $A_{nucleus}$ is the area of the nucleus in the FOV, A_{cell} is the cell area without the nucleus in the FOV, A_{gap} is the gap spaces in the stain slices, and is the overall area of the FOV. The morphological differences were compared by estimating 7 different FOVs for the two cell line tissues.

The significances of different cell lines and indentation strain levels were compared with respect to G_∞ and G_0 with a two-way analysis of variance (ANOVA) test followed by a Bonferroni test with a significance level of .05. A student t-test was used to show the significances of $\phi_{nucleus}$ and ϕ_{cell} with a significance level of .05.

3. Results

A typical force-displacement curve of the indentation test is shown in Fig. 2. To compare the viscoelastic models with different Prony series terms, we fitted a typical indentation curve with Prony series of 1, 2, and 3 terms. We observed that the viscoelastic model with 2 and 3 terms of Prony series provided the best fitting. In fact, the R^2 values for fittings with 1, 2, and 3 terms of Prony series were 0.66, 0.99, and 1.00, respectively. Therefore, we chose the 2-term Prony series for fitting with a minimum number of parameters. Typical fittings of the force-displacement curves at 5 strain levels also showed that the viscoelastic model with 2-term Prony series fitted well, with R^2 values larger than 0.98 for all cases (Fig. 3).

To show the distribution of the experiment data, we normalized the force-displacement curves with respect to the maximum indentation force. The normalized relaxation curves were averaged with standard distribution area plotted for the tissues from 4T1 (Fig. 4) and SKBR (Fig. 5) cell lines. By inspecting the average relaxation curves, we observed that for the 4T1 tissues, it took 2.61 s, 3.73 s, 5.26 s, 6.21 s, and 5.45 s for the indentation force to relax to 60% of its peak force, and 21.25 s, 43.60 s, 69.93 s, 80.47 s, and 64.93 s for 40% relaxation, for strain levels of 2%, 4%, 6%, 8%, and 10%, respectively. For the SKBR3 tissues, the corresponding relaxation time was 1.17 s, 2.99 s, 5.30 s, 7.95 s, and 9.64 s for 60% relaxation, for strain levels of 2%, 4%, 6%, 8%, and 10%, respectively. The relaxation time was 13.10 s, 57.97 s, and 93.39 s for strain levels of 2%, 4%, and 6%, respectively. The average relaxation curve of the SKBR3 tissues could not relax to 40% of the peak indentation force for strain levels of 8% and 10%.

The estimated viscoelastic model parameters for tissue samples from cell lines of 4T1 and SKBR3 are summarized in Tables 1 and 2, respectively. A comparison of the long-term modulus G_∞ showed the cancer tissues from SKBR3 were significantly stiffer than that from 4T1 for all strain levels except 2% (Fig. 6a). However, a comparison of the short-term modulus G_0 showed that the cancer tissues from SKBR3 were not significantly different than that from 4T1 for all strain levels (Fig. 6b). No significant differences of the G_0 values were found across the 5 strain levels for tissues from both cell lines. For the G_∞ values, the only significant differences were observed for 2% indentation with that of 8% and 10%.
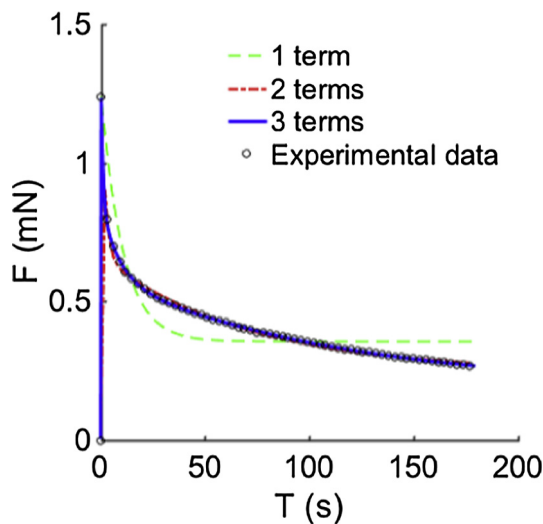
Fig. 2. A typical curve and the fittings of the ramp-hold response from the indentation test with 2% indentation strain. The experiment data was fitted with a viscoelastic model with 1, 2, and 3 terms of Prony series. The corresponding R^2 values were 0.66, 0.99, and 1.00, respectively. Since 2-term Prony series could provide satisfactory fittings, we used 2-term series for fitting all the experiment data.

H&E stain showed that the cancer tissues from 4T1 cell lines were more porous than that of SKBR3 (Fig. 7). The estimated $\phi_{nucleus}$ values were 31.85% ± 6.35% and 46.82% ± 11.93% for 4T1 and SKBR3 tissues, respectively. The estimated ϕ_{cell} values were 66.22% ± 6.26% and 51.42% ± 10.51%, respectively. Both $\phi_{nucleus}$ and ϕ_{cell} values were significantly different between the two cell line tissues (p < .05). These showed that the cancer tissues from 4T1 cell lines have a more scattered distribution of nuclei, with a larger volume ratio of extra cellular matrix.

4. Discussion

In this study, we characterized the mechanical properties of breast cancer tissue from two different cell lines using a mouse model. Using indentation method, we observed significant different viscoelastic properties between the 4T1 and SKBR3 cancer tissues. Comparisons of measured viscoelastic moduli across different strain levels showed largely linear behavior. Analysis of the morphological structures of the cancer tissues showed to be closely related to the mechanical properties of the tissue.

4.1. Elastic and viscoelastic properties

The mechanical properties of the breast cancer tissue have shown to be closely related to its pathologies (Joseph and Samani, 2009; Plodinec et al., 2012; Samani et al., 2007; Sinkus et al., 2005; Umemoto et al., 2014). Samani et al. (2007) were among the very first to investigate the elastic properties of the breast cancer tissue using indentation method. In addition, Umemoto et al. (2014) measured the Young's modulus of the tissues at different stress levels. Although most of the mechanical testing results were from human tissues, this study of the mouse model provides a helpful addition for the animal-based studies. The estimated Young's modulus of the SKBR3 tissues were similar to that of the ductal carcinoma in situ (DCIS) measured with a compression stress of 0–0.2 kPa (Umemoto et al., 2014). Madani and Mojra (2017) used one coefficient of the transfer function of a five-element viscoelastic model to characterize the differences between the healthy and tumor-included regions for human patient. By Laplace transforming Eq. (5) with data from 10% indentation of the SKBR3 tissue, our values were within the range reported but larger than that of the tumor-included regions. This is probably due to the tissue differences and a smaller strain level in our study. The microscale tissue test by Plodinec et al. (2012) using nanoindentation revealed the elastic modulus of malignant breast tissues were ∼0.45 kPa. The difference is largely due to the measurement protocol with differences in testing conditions and a much lower strain level in the microscale.

For instantaneous, elastic response, no significant differences were observed for the G_0 values across the 5 different strain levels. This strain-independent property indicates a linear behavior of the tissue for the short-term responses. For long-term viscoelastic effects, we also observed no significant differences in the G_∞ values for the strain levels of 4–10%. This strain-independent property is desirable for modeling the breast cancer tissue, especially for the elastography measurements based on MRI (Griesenauer et al., 2017; Sinkus et al., 2005) and US (Chang et al., 2013; Coussot et al., 2009; Han et al., 2016; Konofagou et al., 2012; Ophir et al., 2000). In fact, our results provide the first ex vivo measurements to support the linear viscoelastic assumptions of the breast cancer tissue.

Studies have shown that preloading conditions, such as pre-applied stress or strain, could affect the measured properties of the breast cancer tissue (Ramião et al., 2016). When the preloads were applied in terms of strain, significant differences were found
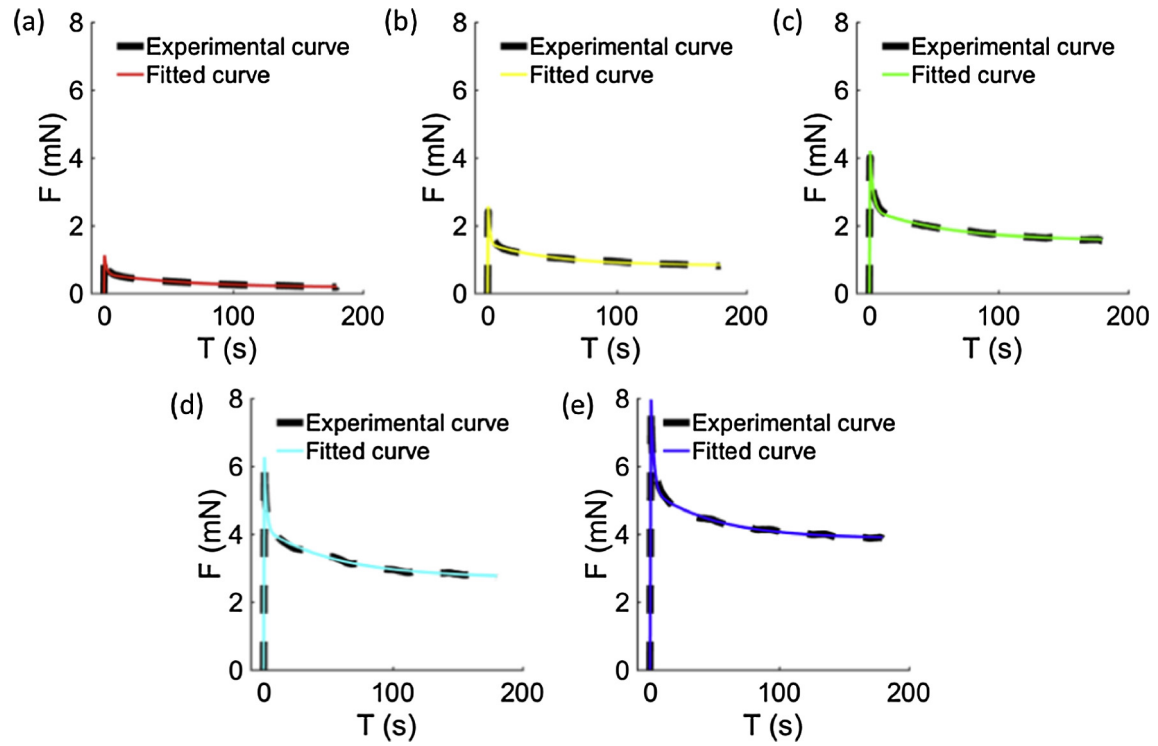
Fig. 3. Typical fitted curves of the ramp-hold responses for indentation strain levels of (a) 2%, (b) 4%, (c) 6%, (d) 8%, and (f) 10%. The R^2 values of the fittings were 0.98, 0.98, 0.98, 0.99, and 0.99, respectively.
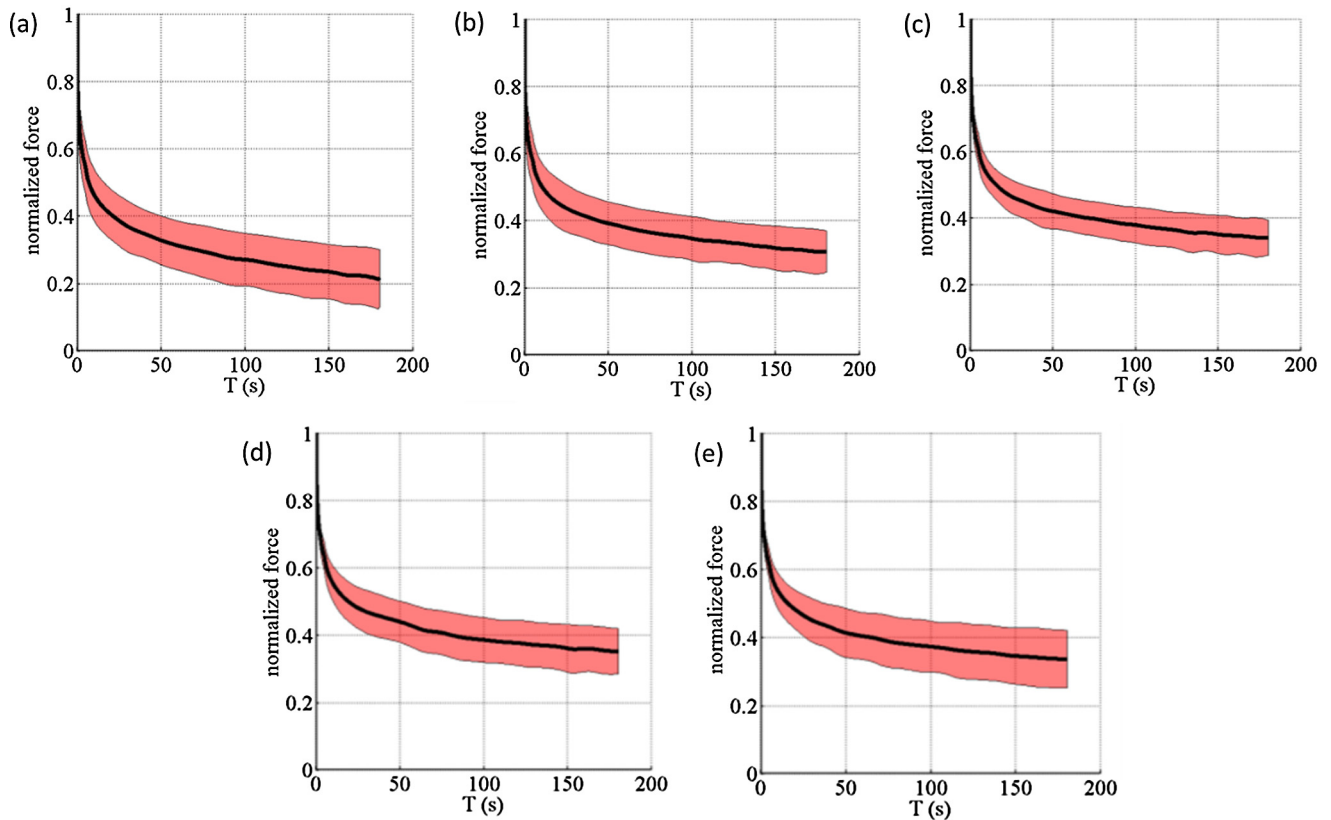
Fig. 4. Average force relaxation curves of the breast cancer tissue from 4T1 cell line. The indentation strain levels were (a) 2%, (b) 4%, (c) 6%, (d) 8%, and (e) 10%. The shaded area indicates the distribution of the measured relaxation curves.
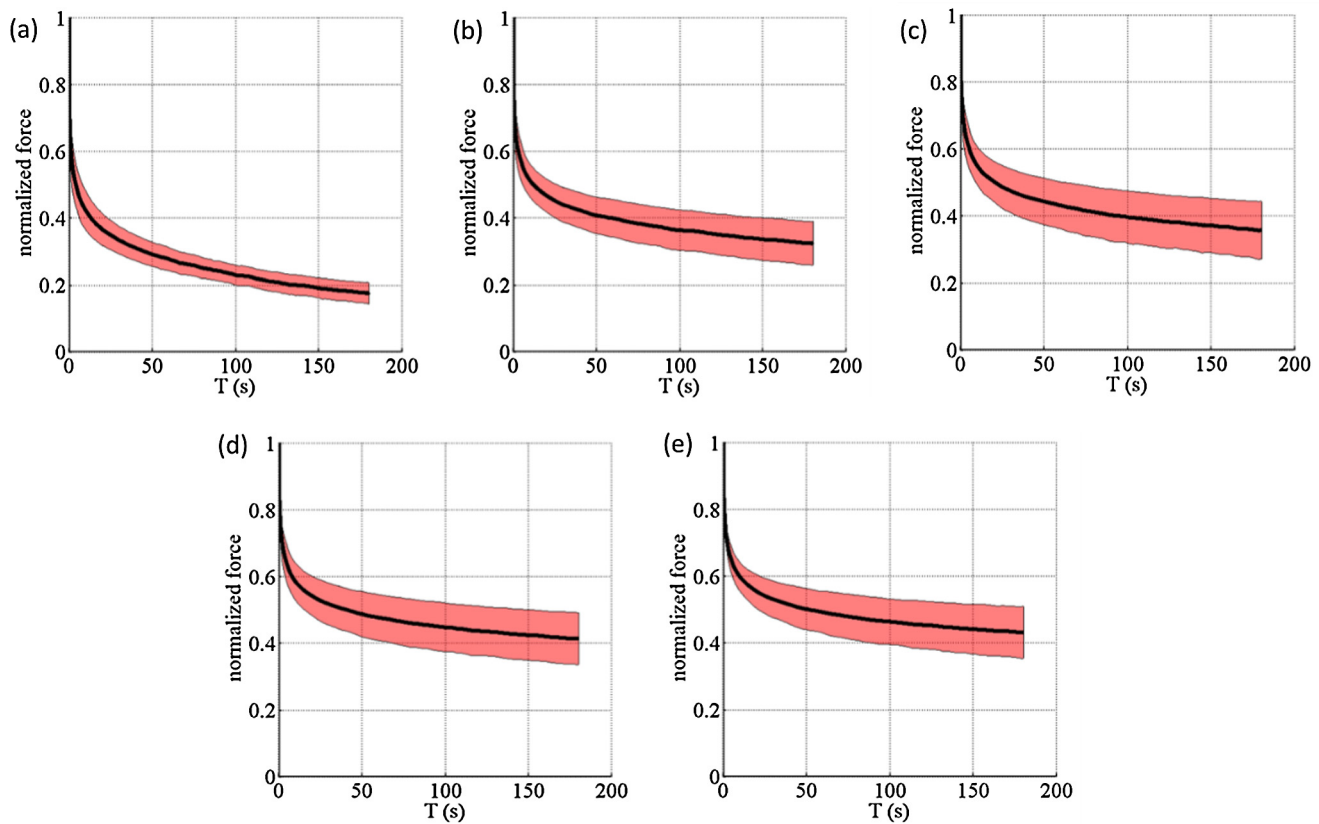
Fig. 5. Average force relaxation curves of the breast cancer tissue from SKBR3 cell line. The indentation strain levels were (a) 2%, (b) 4%, (c) 6%, (d) 8%, and (e) 10%. The shaded area indicates the distribution of the measured relaxation curves.

Table 1
Viscoelastic properties of the breast cancer tissue from 4T1 cell lines with 95% confidence intervals.

| Indentation strain	G_∞ (kPa)	C_1 (kPa)	C_2 (kPa)	τ_1 (s)	τ_2 (s)	G_0 (kPa)	R^2
2%	0.37 ± 0.13	0.98 ± 0.25	0.48 ± 0.03	1.64 ± 0.22	53.14 ± 10.69	1.82 ± 0.32	0.98
4%	0.49 ± 0.05	0.99 ± 0.30	0.40 ± 0.08	1.77 ± 0.22	49.96 ± 3.93	1.89 ± 0.37	0.98
6%	0.52 ± 0.05	0.84 ± 0.23	0.36 ± 0.06	2.49 ± 0.29	54.19 ± 6.44	1.72 ± 0.26	0.98
8%	0.57 ± 0.06	0.85 ± 0.22	0.40 ± 0.07	2.88 ± 0.70	52.68 ± 8.02	1.82 ± 0.25	0.99
10%	0.58 ± 0.09	0.79 ± 0.21	0.51 ± 0.10	8.72 ± 0.94	51.40 ± 10.25	1.88 ± 0.21	0.99

Table 2
Viscoelastic properties of the breast cancer tissue from SKBR3 cell lines with 95% confidence intervals.

| Indentation strain	G_∞ (kPa)	C_1 (kPa)	C_2 (kPa)	τ_1 (s)	τ_2 (s)	G_0 (kPa)	R^2
2%	0.34 ± 0.11	1.30 ± 0.50	0.63 ± 0.27	1.57 ± 0.95	57.38 ± 7.91	2.27 ± 0.84	0.97
4%	0.59 ± 0.16	0.93 ± 0.37	0.42 ± 0.15	2.31 ± 1.13	59.81 ± 9.84	1.94 ± 0.64	0.98
6%	0.60 ± 0.13	0.98 ± 0.47	0.41 ± 0.16	1.82 ± 0.68	52.61 ± 9.56	1.99 ± 0.67	0.98
8%	0.72 ± 0.21	0.75 ± 0.32	0.35 ± 0.13	2.90 ± 0.96	59.12 ± 8.96	1.82 ± 0.62	0.98
10%	0.78 ± 0.20	0.91 ± 0.32	0.38 ± 0.15	2.00 ± 0.60	49.79 ± 7.63	2.07 ± 0.63	0.98

for the measured elastic modulus between the strain range of 1–5% and 15–20% (Krouskop et al., 1998). This demonstrates a nonlinear behavior in the large strain regime, as many other biological tissues have shown (Feng et al., 2016, 2013). In this study, we did observe an increase of G_∞ value for both tissues as the strain level increased. In addition, the only significant differences of the G_∞ values were observed for 2% vs. 8% and 2% vs. 10%, which showed an gradually emerging nonlinear effect as the strain transits from small to large. Although we focused on a relatively low strain level for characterization, it is expected that a larger increase of modulus for larger deformations.

By comparing the relaxation time of 60% of the peak indentation force, we observed that the 4T1 tissue had a longer mean relaxation time than that of SKBR3 at 2% and 4% strain (Fig. 8). However, for strains larger than 4%, the trend reversed. Although no significant differences were found between the two cell lines, significant differences of the 60% relaxation time were found for the 2% vs. 8% and 2% vs. 10% strain levels. Similar differences were also observed for the G_∞ values. The different responses at 6–10% strain indicate that as the strain level increases, it is suggested to take into consideration of the time-domain nonlinear effect for viscoelastic modeling of the cancer tissue.
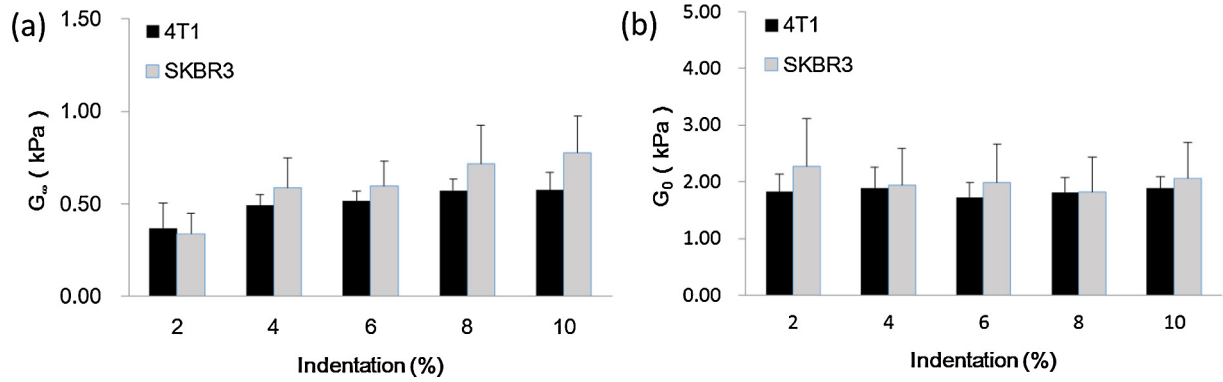
Fig. 6. Comparisons of (a) long term shear modulus G_∞ and (b) instantaneous shear modulus G_0 of the cancer tissues from 4T1 and SKBR3 cell lines for each indentation strain level (mean ± 95% confidence interval). A two-way ANOVA test followed by a Bonferroni test showed that G_∞ was significantly different between tissues from the two cell lines ($p < .05$). The only significant differences found between indentation strain levels were 2% vs. 8% and 2% vs. 10% ($p < .05$).
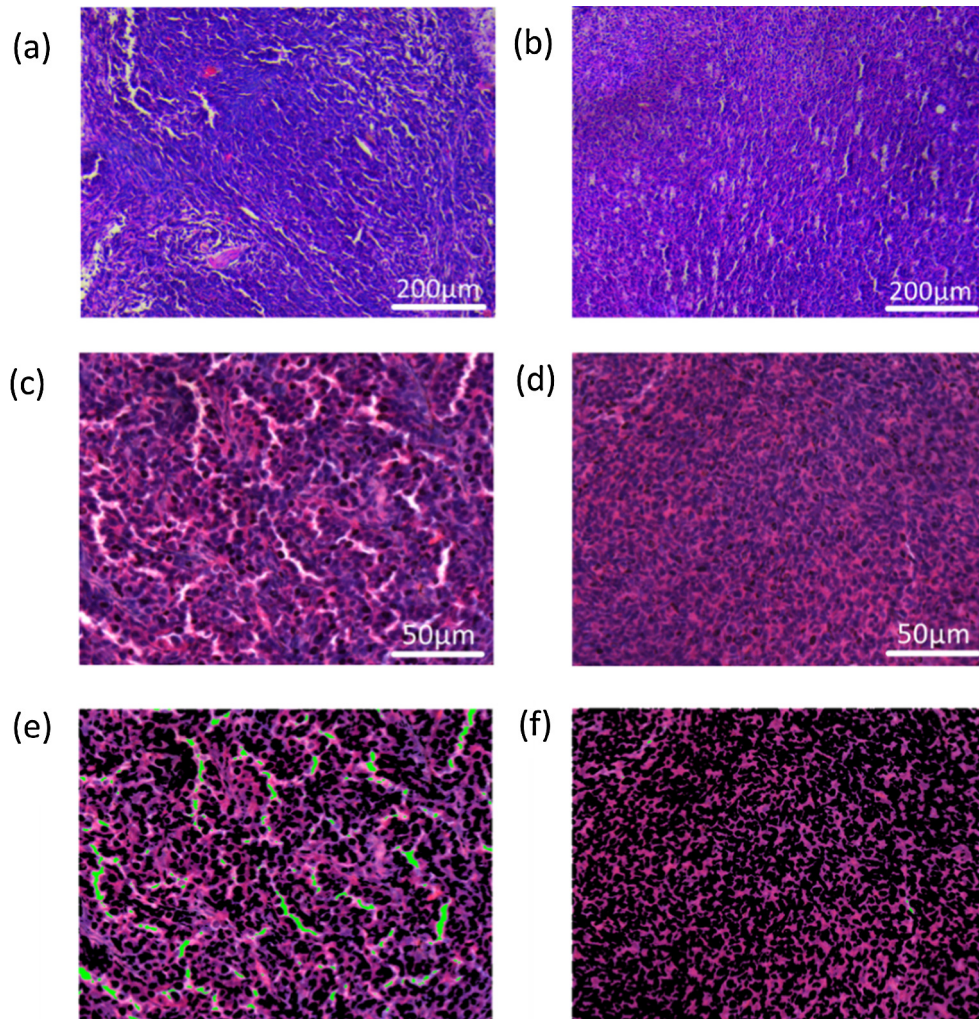

Fig. 7. H&E staining of the cancer tissues from (a, c) 4T1 and (b, d) SKBR3 cell lines with a magnification level of 10× and 40×, respectively. The gap spaces of the stain slices and the nuclei region were marked with green and dark colors for the (e) 4T1 and (f) SKBR3 tissues, respectively. The $\phi_{nucleus}$ and ϕ_{cell} values for the 4T1 and SKBR3 tissues were 33.23% and 63.30%, 40.22% and 44.49%, respectively. (For interpretation of the references to colour in this figure legend, the reader is referred to the web version of this article.)

4.2. Viscoelastic model

Based on different measurement modalities, different viscoelastic models have been proposed to model the mechanical behavior of breast cancer tissue. Sinkus et al. (2005) proposed the first anisotropic model with viscoelastic properties incorporated, where a single viscosity term was used to describe the viscoelastic behavior of the tissue. Coussot et al. (2009) showed a viscoelastic model with only three terms could be used to characterize the cancer tissue. In this study, we showed that the 2-term Prony series were
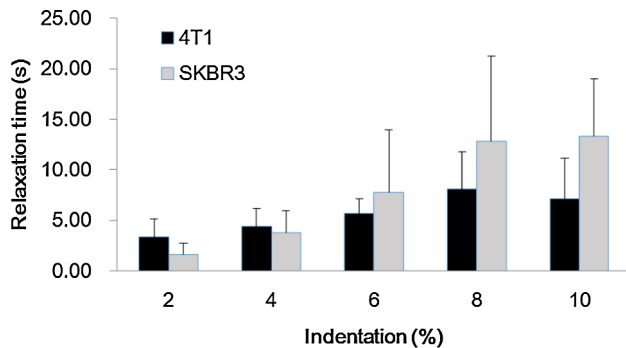
Fig. 8. A comparison of relaxation time of 60% of the peak indentation force between the 4T1 and SKBR3 tissues (mean ± 95% confidence interval). A two-way ANOVA test showed no significant differences between the two tissues. However, significant differences were found for 2% vs. 8%, and 2% vs. 10% indentation strains (p < .05).

good enough to describe the viscoelastic behavior of the breast cancer tissue. From a physical point of view, the single viscosity model is equivalent to the standard Kelvin model, the 2-term Prony series is equivalent to the five-element Maxwell-Wiechert model (Madani and Mojra, 2017), and the 3-term Prony series is equivalent to a Triple Maxwell-arm Wiechert model (Wang et al., 2013). Since the application scenario always requires model simplification and modification, our results provided an ex vivo characterization that is useful for guiding the model selection and modification.

4.3. Correlation with morphological structures

Cellular level studies of the breast cancer cells showed that Young's modulus ranged from 0.3 to 1 kPa (Li et al., 2008; Omidvar et al., 2014). These were much lower than the elastic modulus measured at the tissue level. These results imply that the mechanical properties of the extra cellular matrix (ECM) may play a major role in the macroscopic mechanical response of the breast cancer tissue. In fact, the roles of ECM in mechanobiology and mechanotransduction are known for keeping the tissue-level structure and functionality (Humphrey et al., 2014; Mouw et al., 2014). By inspecting the morphological differences in the cellular level, we observed a higher nuclei density in the SKBR3 tissue than that of 4T1. However, a lower ϕ_{cell} value indicates SKBR3 tissue had a lower volume ratio of the ECM. These indicated that the ECM in SKBR3 tissue embedding more densely populate cells may have a higher stiffness than that of 4T1 tissues with loosely distributed cells. These results could provide helpful information for modeling the multiscale cell-tissue mechanical behavior.

4.4. Limitations and future studies

Although we acquired the sample tissues by keeping the same dimensions of the solid tumor mass on the mice legs, it is hard to precisely control the tumor growth at the same stage. This could contribute to variations of mechanical properties of the tumor tissue. In addition, although we tried to moisturize the sample during the test, it is hard to control and keep the moisture of the sample at the same level. Finally, an assumption of tissue homogeneity was adopted in the characterization that could also contribute to the estimation errors. Future studies include a correlation study between the indentation measurements and the elastography method, applications to clinical tissue samples, and mechanotransduction studies of the cancer treatment evaluation.

5. Conclusions

A custom-built indentation device with ramp-hold stress relaxation tests was used to characterize the viscoelastic properties of breast cancer tissues from two different cell lines. By analyzing the force ramp and relaxation of the indentation, we found the 2-term Prony series could best fit the experimental data. Estimate of the viscoelastic properties showed cancer tissues from SKBR3 cell line had significant larger long-term shear modulus than that of 4T1 cell line for indentation strains of 4–10%. However, measured shear moduli were mostly strain-independent for both cancer tissues. Investigation of the cellular morphological structure of the two tissues showed the SKBR3 tissues had a larger volume ratio of nuclei and a smaller volume ratio of ECM, indicating ECM could contribute to the stiffening of the tissue-level behavior. Our results could help a phenomenological modeling of the breast cancer in the tissue level and could provide helpful insights into the modeling at the cellular levels. The viscoelastic behavior characterized could also help validating and improving image-based elastography method for breast cancer tissues.

Conflict of interest statement

No conflict of interest exists.

References

Ahn, B.-M., Kim, J., Ian, L., Rha, K.-H., Kim, H.-J., 2010. Mechanical property characterization of prostate cancer using a minimally motorized indenter in an ex vivo indentation experiment. Urology 76, 1007–1011.

Babaei, B., Abramowitch, S.D., Elson, E.L., Thomopoulos, S., Genin, G.M., 2015a. A discrete spectral analysis for determining quasi-linear viscoelastic properties of biological materials. Journal of the Royal Society, Interface / the Royal Society 12.

Babaei, B., Davarian, A., Pryse, K.M., Elson, E.L., Genin, G.M., 2015b. Efficient and optimized identification of generalized Maxwell viscoelastic relaxation spectra. J. Mech. Behav. Biomed. Mater. 55, 32–41.

Budday, S., Nay, R., de Rooij, R., Steinmann, P., Wyrobek, T., Ovaert, T.C., Kuhl, E., 2015. Mechanical properties of gray and white matter brain tissue by indentation. J. Mech. Behav. Biomed. 46, 318–330.

Chang, J.M., Won, J.-K., Lee, K.-B., Park, I.A., Yi, A., Moon, W.K., 2013. Comparison of shear-wave and strain ultrasound elastography in the differentiation of benign and malignant breast lesions. Am. J. Roentgenol. 201, W347–W356.

Coussot, C., Kalyanam, S., Yapp, R., Insana, M.F., 2009. Fractional derivative models for ultrasonic characterization of polymer and breast tissue viscoelasticity. IEEE Trans. Ultrason. Ferroelectr. Freq. Control 56, 715–726.

Darling, E.M., Zauscher, S., Guilak, F., 2006. Viscoelastic properties of zonal articular chondrocytes measured by atomic force microscopy. Osteoarthritis Cartilage 14, 571–579.

Dimitriadis, E.K., Horkay, F., Maresca, J., Kachar, B., Chadwick, R.S., 2002. Determination of elastic moduli of thin layers of soft material using the atomic force microscope. Biophys. J . 82, 2798–2810.

Elkin, B.S., Ilankova, A., Morrison, B., 2011. Dynamic, regional mechanical properties of the porcine brain: indentation in the coronal plane. J. Biomech. Eng.-Trans, 133.

Feng, Y., Gao, Y., Wang, T., Tao, L., Qiu, S., Zhao, X., 2017a. A longitudinal study of the mechanical properties of injured brain tissue in a mouse model. J. Mech. Behav. Biomed. 71, 407–415.

Feng, Y., Lee, C.-H., Sun, L., Ji, S., Zhao, X., 2017b. Characterizing white matter tissue in large strain via asymmetric indentation and inverse finite element modeling. J. Mech. Behav. Biomed. 65, 490–501.

Feng, Y., Okamoto, R.J., Genin, G.M., Bayly, P.V., 2016. On the accuracy and fitting of transversely isotropic material models. J. Mech. Behav. Biomed. 61, 554–566.

Feng, Y., Okamoto, R.J., Namani, R., Genin, G.M., Bayly, P.V., 2013. Measurements of mechanical anisotropy in brain tissue and implications for transversely isotropic material models of white matter. J. Mech. Behav. Biomed. 23, 117–132.

Fischer-Cripps, A.C., 2000. Introduction to Contact Mechanics. Springer.

Gang, Z., Qi, Q., Jing, C., Wang, C., 2009. Measuring microenvironment mechanical stress of rat liver during diethylnitrosamine induced hepatocarcinogenesis by atomic force microscope. Microsc. Res. Tech. 72, 672–678.

Griesenauer, R.H., Weis, J.A., Arlinghaus, L.R., Meszoely, I.M., Miga, M.I., 2017. Breast tissue stiffness estimation for surgical guidance using gravity-induced excitation. Phys. Med. Biol. 62, 4756–4776.

Han, B., Nia, H.T., Wang, C., Chandrasekaran, P., Li, Q., Chery, D.R., Li, H., Grodzinsky, A.J., Han, L., 2017. AFM-nanomechanical test: an interdisciplinary tool that links the understanding of cartilage and meniscus biomechanics, osteoarthritis degeneration, and tissue engineering. ACS Biomater. Sci. Eng. 3, 2033–2049.

Han, Y., Wang, S., Hibshoosh, H., Taback, B., Konofagou, E., 2016. Tumor characterization and treatment monitoring of postsurgical human breast specimens using harmonic motion imaging (HMI). Breast Cancer Res. 18, 46.

Hipwell, J.H., Vavourakis, V., Han, L.H., Mertzanidou, T., Eiben, B., Hawkes, D.J., 2016. A review of biomechanically informed breast image registration. Phys. Med. Biol. 61, R1–R31.

Hosseini, S.M., Kashani, S.M., Najarian, S., Panahi, F., Naeini, S.M., Mojra, A., 2010. A medical tactile sensing instrument for detecting embedded objects, with specific application for breast examination. Int. J. Med. Robot. + Comput. Assisted Surg.: MRCAS 6, 73–82.

Humphrey, J.D., Dufresne, E.R., Schwartz, M.A., 2014. Mechanotransduction and extracellular matrix homeostasis. Nat. Rev. Mol. Cell Biol. 15, 802–812.

Jain, R.K., Martin, J.D., Stylianopoulos, T., 2014. The role of mechanical forces in tumor growth and therapy. Annu. Rev. Biomed. Eng. 16, 321–346.

Jemal, A., Bray, F., Center, M.M., Ferlay, J., Ward, E., Forman, D., 2011. Global cancer statistics. CA Cancer J. Clin. 61, 69–90.

Joseph, J.O.H., Samani, A., 2009. Measurement of the hyperelastic properties of 44 pathological ex vivo breast tissue samples. Phys. Med. Biol. 54, 2557.

Konofagou, E.E., Maleke, C., Vappou, J., 2012. Harmonic motion imaging (HMI) for tumor imaging and treatment monitoring. Curr. Med. Imaging Rev. 8, 16–26.

Krouskop, T.A., Wheeler, T.M., Kallel, F., Garra, B.S., Hall, T., 1998. Elastic moduli of breast and prostate tissues under compression. Ultrasonic Imaging 20, 260–274.

Li, Q., Qu, F., Han, B., Wang, C., Li, H., Mauck, R.L., Han, L., 2017. Micromechanical anisotropy and heterogeneity of the meniscus extracellular matrix. Acta Biomater. 54, 356–366.

Li, Q.S., Lee, G.Y.H., Ong, C.N., Lim, C.T., 2008. AFM indentation study of breast cancer cells. Biochem. Biophys. Res. Commun. 374, 609–613.

MacManus, D.B., Pierrat, B., Murphy, J.G., Gilchrist, M.D., 2016. Mechanical characterization of the P56 mouse brain under large-deformation dynamic indentation. Sci. Rep. 6, 21569.

Madani, N., Mojra, A., 2017. Quantitative diagnosis of breast tumors by characterization of viscoelastic behavior of healthy breast tissue. J. Mech. Behav. Biomed. 68, 180–187.

Mariappan, Y.K., Glaser, K.J., Manduca, A., Romano, A.J., Venkatesh, S.K., Yin, M., Ehman, R.L., 2009. High-frequency mode conversion technique for stiff lesion detection with magnetic resonance elastography (MRE). Magn. Reson. Med. 62, 1457–1465.

Mattice, J.M., Lau, A.G., Oyen, M.L., Kent, R.W., 2006. Spherical indentation load-relaxation of soft biological tissues. J. Mater. Res. 21, 2003–2010.

Mojra, A., Najarian, S., Kashani, S.M.T., Panahi, F., 2012. A novel tactile-guided detection and three-dimensional localization of clinically significant breast masses. J. Med. Eng. Technol. 36, 8–16.

Mojra, A., Najarian, S., Towliat Kashani, S.M., Panahi, F., Yaghmaei, M., 2011. A novel haptic robotic viscogram for characterizing the viscoelastic behaviour of breast tissue in clinical examinations. Int. J. Med. Robot. + Comput. Assisted Surg.: MRCAS 7, 282–292.

Moustris, G.P., Hiridis, S.C., Deliparaschos, K.M., Konstantinidis, K.M., 2011. Evolution of autonomous and semi-autonomous robotic surgical systems: a review of the literature. Int. J. Med. Robot. + Comput. Assisted Surg.: MRCAS 7, 375–392.

Mouw, J.K., Ou, G., Weaver, V.M., 2014. Extracellular matrix assembly: a multiscale deconstruction. Nat. Rev. Mol. Cell Biol. 15, 771–785.

Nia, H.T., Liu, H., Seano, G., Datta, M., Jones, D., Rahbari, N., Incio, J., Chauhan, V.P., Jung, K., Martin, J.D., Askoxylakis, V., Padera, T.P., Fukumura, D., Boucher, Y., Hornicek, F.J., Grodzinsky, A.J., Baish, J.W., Munn, L.L., Jain, R.K., 2016. Solid stress and elastic energy as measures of tumour mechanopathology. Nat. Biomed. Eng., 1

Ning, X., Zhu, Q., Lanir, Y., Margulies, S.S., 2006. A transversely isotropic viscoelastic constitutive equation for brainstem undergoing finite deformation. J. Biomech. Eng. 128, 925–933.

Omidvar, R., Tafazzoli-shadpour, M., Shokrgozar, M.A., Rostami, M., 2014. Atomic force microscope-based single cell force spectroscopy of breast cancer cell lines: an approach for evaluating cellular invasion. J. Biomech. 47, 3373–3379.

op den Buijs, J., Hansen, H.H., Lopata, R.G., de Korte, C.L., Misra, S., 2011. Predicting target displacements using ultrasound elastography and finite element modeling. IEEE Trans. Bio-med. Eng. 58, 3143–3155.

Ophir, J., Garra, B., Kallel, F., Konofagou, E., Krouskop, T., Righetti, R., Varghese, T., 2000. Elastographic imaging. Ultrasound Med. Biol. 26 (Suppl 1), S23–29.

Oyen, M.L., 2005. Spherical indentation creep following ramp loading. J. Mater. Res. 20, 2094–2100.

Park, S., Costa, K.D., Ateshian, G.A., 2004. Microscale frictional response of bovine articular cartilage from atomic force microscopy. J. Biomech. 37, 1679–1687.

Pathmanathan, P., Gavaghan, D.J., Whiteley, J.P., Chapman, S.J., Brady, J.M., 2008. Predicting tumor location by modeling the deformation of the breast. IEEE Trans. Bio-med. Eng. 55, 2471–2480.

Plodinec, M., Loparic, M., Monnier, C.A., Obermann, E.C., Zanetti-Dallenbach, R., Oertle, P., Hyotyla, J.T., Aebi, U., Bentires-Alj, M., Lim, R.Y., 2012. The nanomechanical signature of breast cancer. Nature Nanotechnol. 7, 757–765.

Qiang, B., Greenleaf, J., Oyen, M., Zhang, X., 2011. Estimating material elasticity by spherical indentation load-relaxation tests on viscoelastic samples of finite thickness. IEEE Trans. Ultrason. Ferroelectr. Freq. Control 58, 1418–1429.

Raghupathy, R., Barocas, V.H., 2010. Generalized anisotropic inverse mechanics for soft tissues. J. Biomech. Eng. 132, 081006.

Ramião, N.G., Martins, P.S., Rynkevic, R., Fernandes, A.A., Barroso, M., Santos, D.C., 2016. Biomechanical properties of breast tissue, a state-of-the-art review. Biomech. Model. Mechanobiol. 15, 1307–1323.

Samani, A., Bishop, J., Luginbuhl, C., Plewes, D.B., 2003. Measuring the elastic modulus of ex vivo small tissue samples. Phys. Med. Biol. 48, 2183.

Samani, A., Zubovits, J., Plewes, D., 2007. Elastic moduli of normal and pathological human breast tissues: an inversion-technique-based investigation of 169 samples. Phys. Med. Biol. 52, 1565.

Schierbaum, N., Rheinlaender, J., Schäffer, T.E., 2017. Viscoelastic properties of normal and cancerous human breast cells are affected differently by contact to adjacent cells. Acta Biomater. 55, 239–248.

Siegel, R.L., Miller, K.D., Jemal, A., 2016. Cancer statistics, 2016. CA Cancer J. Clin. 66, 7–30.

Sinkus, R., Tanter, M., Xydeas, T., Catheline, S., Bercoff, J., Fink, M., 2005. Viscoelastic shear properties of in vivo breast lesions measured by MR elastography. Magn. Reson. Imaging 23, 159–165.

Stylianopoulos, T., Martin, J.D., Chauhan, V.P., Jain, S.R., Diop-Frimpong, B., Bardeesy, N., Smith, B.L., Ferrone, C.R., Hornicek, F.J., Boucher, Y., 2012. Causes, consequences, and remedies for growth-induced solid stress in murine and human tumors. Proc. Natl. Acad. Sci. 109, 15101–15108.

Toohey, K.S., Kalyanam, S., Palaniappan, J., Insana, M.F., 2016. Indentation analysis of biphasic viscoelastic hydrogels. Mech. Mater. Int. J. 92, 175–184.

Tyagi, M., Wang, Y., Hall, T.J., Barbone, P.E., Oberai, A.A., 2017. Improving three-dimensional mechanical imaging of breast lesions with principal component analysis. Med. Phys. 44, 4194–4203.

Umemoto, T., Ueno, E., Matsumura, T., Yamakawa, M., Bando, H., Mitake, T., Shiina, T., 2014. Ex vivo and in vivo assessment of the non-linearity of elasticity properties of breast tissues for quantitative strain elastography. Ultrasound Med. Biol. 40, 1755–1768.

van Dommelen, J.A.W., van der Sande, T.P.J., Hrapko, M., Peters, G.W.M., 2010. Mechanical properties of brain tissue by indentation: interregional variation. J. Mech. Behav. Biomed. 3, 158–166.

Wang, X., Schoen, J.A., Rentschler, M.E., 2013. A quantitative comparison of soft tissue compressive viscoelastic model accuracy. J. Mech. Behav. Biomed. 20, 126–136.

Wex, C., Stoll, A., Frohlich, M., Arndt, S., Lippert, H., 2014. Mechanics of fresh, frozen-thawed and heated porcine liver tissue. Int. J. Hyperthermia 30, 271–283.

Wirtz, D., Konstantopoulos, K., Searson, P.C., 2011. The physics of cancer: the role of physical interactions and mechanical forces in metastasis. Nat. Rev. Cancer 11, 512–522.

Zhang, M.G., Cao, Y.P., Li, G.Y., Feng, X.Q., 2014. Spherical indentation method for determining the constitutive parameters of hyperelastic soft materials. Biomech. Model. Mechanobiol. 13, 1–11.

Zhang, W., Feng, Y., Lee, C.-H., Billiar, K.L., Sacks, M.S., 2015. A generalized method for the analysis of planar biaxial mechanical data using tethered testing configurations. J. Biomech. Eng. 137. 064501–064501.